The Relationship between High-Presentation Asthma Days in Melbourne, Australia, and Modeled Thunderstorm Environments

ANDREW BROWN,[a] ANDREW DOWDY,[a] AND ELIZABETH E. EBERT[a]

[a] *Bureau of Meteorology, Melbourne, Victoria, Australia*

(Manuscript received 1 July 2021, in final form 30 November 2021)

ABSTRACT: Epidemic asthma events represent a significant risk to emergency services as well as the wider community. In southeastern Australia, these events occur in conjunction with relatively high amounts of grass pollen during the late spring and early summer, which may become concentrated in populated areas through atmospheric convergence caused by a number of physical mechanisms including thunderstorm outflow. Thunderstorm forecasts are therefore important for identifying epidemic asthma risk factors. However, the representation of thunderstorm environments using regional numerical weather prediction models, which are a key aspect of the construction of these forecasts, have not yet been systematically evaluated in the context of epidemic asthma events. Here, we evaluate diagnostics of thunderstorm environments from historical simulations of weather conditions in the vicinity of Melbourne, Australia, in relation to the identification of epidemic asthma cases based on hospital data from a set of controls. Skillful identification of epidemic asthma cases is achieved using a thunderstorm diagnostic that describes near-surface water vapor mixing ratio. This diagnostic is then used to gain insights on the variability of meteorological environments related to epidemic asthma in this region, including diurnal variations, long-term trends, and the relationship with large-scale climate drivers. Results suggest that there has been a long-term increase in days with high water vapor mixing ratio during the grass pollen season, with large-scale climate drivers having a limited influence on these conditions.

SIGNIFICANCE STATEMENT: We investigate the atmospheric conditions associated with epidemic thunderstorm asthma events in Melbourne, Australia, using historical model simulations of the weather. Conditions appear to be associated with high atmospheric moisture content, which relates to environments favorable for severe thunderstorms, but also potentially pollen rupturing as suggested by previous studies. These conditions are shown to be just as important as the concentration of grass pollen for a set of epidemic thunderstorm asthma events in this region. This means that weather model simulations of thunderstorm conditions can be incorporated into the forecasting process for epidemic asthma in Melbourne, Australia. We also investigate long-term variability in atmospheric conditions associated with severe thunderstorms, including relationships with the large-scale climate and long-term trends.

KEYWORDS: Storm environments; Thunderstorms; Reanalysis data; Regional models; Interannual variability; Health

1. Introduction

Epidemic asthma events have the potential to place a large strain on emergency service networks and can lead to dangerous situations for susceptible members of society (Thien et al. 2018). Major asthma events of this nature have occurred once every few years in southeastern Australia (Price et al. 2021) and have in some cases been shown to relate to thunderstorm occurrences in the presence of high grass pollen concentrations (Bellomo et al. 1992; Marks et al. 2001). Although the exact mechanisms which lead to epidemic asthma events remain unclear, it is thought that atmospheric convergence can cause pollen to become highly concentrated in populated areas (Bannister et al. 2020), with thunderstorms being an efficient producer of localized convergence due to strong surface outflow. However, there are also a wide range of complex factors which then relate pollen exposure to asthma, including the duration of exposure, the presence of other allergens and background grass pollen concentrations, social factors and other disease entities (Davies et al. 2017). In addition to concentrating pollen due to surface convergence, deep moist convection may potentially provide a pollen rupturing process through high moisture content, lightning, or strong winds, for example, which is a likely requirement for epidemic asthma events (Taylor and Jonsson 2004; Emmerson et al. 2021).

After a catastrophic thunderstorm asthma event occurred in Melbourne, Australia in November 2016 (see Thien et al. 2018 for details), a forecast service was commissioned for the state of Victoria, which has been running since 2017 (Bannister et al. 2021). Forecasts are issued with a maximum lead time of 2 days, based on two primary factors; concentration of grass pollen and potential for severe thunderstorms with strong outflow, characterized by damaging winds greater than 25 m s^{-1} as indicated by Australian Bureau of Meteorology forecasters. The severe thunderstorm aspect of this forecast incorporates the usual tools available to an extreme weather forecaster (Sgarbossa et al. 2019), such as details of the atmospheric environment provided by observations and global or

Denotes content that is immediately available upon publication as open access.

Corresponding author: Andrew Brown, andrew.brown@bom.gov.au

DOI: 10.1175/WAF-D-21-0109.1

mesoscale numerical weather prediction (NWP) models, as well as high-resolution convection-permitting models, with radar and satellite providing insights for shorter lead times.

As part of this forecasting process, atmospheric environments which are favorable for severe thunderstorm occurrence are identified, often using severe weather diagnostics or indices (Doswell and Schultz 2006). These diagnostics typically form an ingredients-based approach, which indicate where and when there is moisture and instability available for deep moist convection, with differences in wind speed and/or direction with height often incorporated to indicate potential for convective organization, which may lead to longer-lived systems with enhanced impacts (Weisman and Klemp 1982). In addition, diagnostics have been developed to identify thunderstorm environments with strong downdrafts and enhanced severe wind potential, which may be potentially relevant for epidemic asthma events, noting that severe winds can occur in a range of different environments (Wakimoto 2001). Other diagnostics represent environments favorable for certain convective modes, which may have regions of strong downdrafts and outflow (Schumacher and Rasmussen 2020). Enhanced severe wind potential as inferred from the atmospheric environment, derived from global model data, has been associated with previous asthma epidemics in southeastern Australia, such as the November 2016 event (Grundstein et al. 2017). However, the relationship between thunderstorm environments from regional model data and epidemic asthma events has yet to be tested in a systematic way.

In addition to forecasting challenges, there are also large uncertainties surrounding the long-term variability of thunderstorm asthma events, in particular relating to the potential influence of climate change on grass pollen and severe thunderstorms. While several studies have reported increasing pollen concentrations and/or allergenicity with global temperature increases (Beggs 2004; Anderegg et al. 2021), de Morton et al. (2011) showed that grass pollen concentrations in the Melbourne region have been in decline over recent decades, related to declines in winter–spring rainfall and land use changes. In a recent review paper, Thien et al. (2020) have suggested that grass pollen variability in southeast Australia could also be related to large-scale climate drivers such as El Niño Southern Oscillation, based on conditions leading up to the November 2016 Melbourne event (Thien et al. 2018). In addition to pollen concentrations, recent studies have also shown that environments favorable for severe thunderstorms have changed in frequency in some regions of the world (Taszarek et al. 2021) and may increase in frequency under climate change due to increasing atmospheric moisture content and convective instability (Trapp et al. 2007; Allen et al. 2014). However, there are large uncertainties in the details in these future projections, including for individual thunderstorm hazards, changes in their intensity and regional changes (Allen 2018), as well as for their potential impacts on public health.

Here, we investigate a range of severe weather diagnostics for a set of high hospital presentation asthma cases in Melbourne, Australia, with an assessment of skill against a set of control days. This includes diagnostics intended to indicate severe wind potential associated with thunderstorm outflow or certain convective modes, as well as diagnostics intended to identify severe thunderstorm environments more generally. Diagnostics are derived from the Australian Bureau of Meteorology ("Bureau") Atmospheric Regional Reanalysis for Australia (BARRA: Su et al. 2019), which is a historical simulation based on a similar dynamical model to the Bureau's regional NWP model (the Australian Community Climate and Earth-System Simulator (ACCESS; Puri et al. 2013), used as part of the thunderstorm asthma forecast service as described above. In addition, a global reanalysis (ERA5; Hersbach et al. 2020) is also used to account for potential model uncertainties. The skill of severe weather diagnostics in identifying asthma case days will also be compared with the equivalent skill using grass pollen data only. Lower-tropospheric water vapor mixing ratio is shown to have significant skill based on case/control analysis and is then analyzed over a long period (1991–2018), to provide insights on variability in favorable meteorological conditions for epidemic asthma events in this region. Moisture variability is compared with long-term variability in grass pollen concentrations, and large-scale climate drivers relevant for southeastern Australia.

2. Method

a. High hospital presentation asthma case and control days

High hospital presentation asthma case days are identified for Melbourne using the same definition as Bannister et al. (2020). A daily time series of asthma presentations are obtained for 20 public hospitals in the Melbourne region during the period 2009–17, in a 75-km radius centered on the Laverton weather radar (Fig. 1). Each day is defined as spanning from 1200 local time (LT) to 1200 LT the following day. High hospital presentation asthma case days are defined when there are at least 10 presentations at any given hospital, and control days are defined by all null case days in the period. A threshold of 10 presentations in a 24-h period was chosen based on the frequency distribution of presentations, with numbers greater than 10 occurring either once or less over the 2009–17 period at each hospital (Bannister et al. 2020). In addition, all case and control dates are restricted to the grass pollen season in this region (1 October–31 December; de Morton et al. 2011), with the resulting dataset containing 21 cases and 807 controls.

b. Meteorological data

The meteorological data used here include severe weather diagnostics computed from the Bureau Atmospheric Regional Reanalysis for Australia (BARRA; Su et al. 2019) and the ERA5 global reanalysis (Hersbach et al. 2020). The diagnostics are chosen based on a survey of severe weather literature and operational forecasting practices, noting that some of the diagnostics here have been applied to weather model data by previous studies, and are hypothesized to be associated with asthma epidemics in this region (Grundstein et al. 2017) as well as severe thunderstorm winds in Australia (Brown and Dowdy

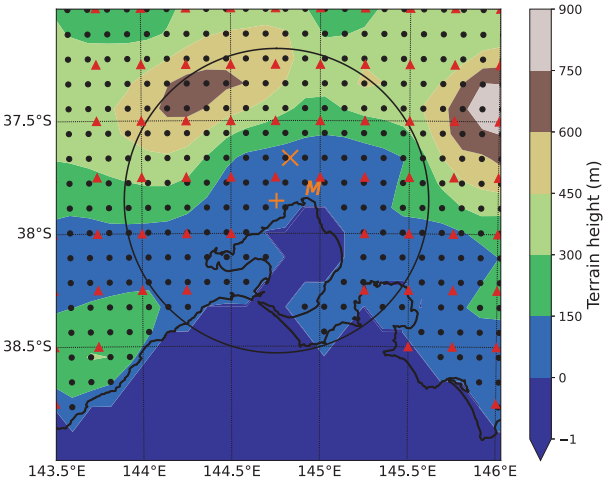

FIG. 1. Map showing the 75-km radius around Laverton airport radar (labeled "+"), used to define the area for health data and the spatial summary area from BARRA and ERA5. The location of the pollen counting instrument at the University of Melbourne is also shown ("M"). The location where Melbourne airport rawinsondes are launched is marked with a cross. Terrain height used by the BARRA reanalysis is shown with shaded contours, with BARRA grid points also indicated by black circles and ERA5 grid points represented by red triangles (model land points only).

2021). Formulations of severe weather diagnostics are shown in Table 1, along with the appropriate references. Multiple Python packages were used for the calculation of severe weather diagnostics (Blumberg et al. 2017; Ladwig 2017; May et al. 2019).

Both reanalysis datasets have hourly data, as used in this study for calculating severe weather diagnostics, which are considered instantaneous unless noted otherwise in Table 1. ERA5 has horizontal grid spacing of 0.25° in latitude and longitude on 37 pressure levels (27 of which are at or below 100 hPa), whereas BARRA data has horizontal grid spacing of 0.11° (37 pressure levels, 22 levels below 100 hPa). As well as pressure level data, surface level data are included in the calculation of each diagnostic. After the diagnostics have been calculated, the spatial maximum is taken over the same 75-km radius as was used for the case and control data, using model land points only (Fig. 1). The hourly diagnostics are then resampled to daily maximum values, for comparison with daily asthma data. Daily and spatial maxima were computed to account for the relatively short durations and potentially small spatial scales of thunderstorm events. For each day, hourly model values from 0100 to 0000 UTC at the start of the next day are used, corresponding to the temporal window used to define case and control days (LT in this region is UTC + 11 hours including + 1 h daylight savings through October–December). For investigating long-term variability of thunderstorm environments and correlations with large-scale climate drivers, data are used from 1991 to 2018 from BARRA and ERA5, with this period chosen based on the availability of BARRA (1990–2018) and grass pollen data (1991–2020; section 2c).

BARRA and ERA5 each use models that have parameterized convection, in which thunderstorm-related environments are reasonably represented in southeastern Australia (Brown and Dowdy 2021). However, there is considerable variability in model representations between convective diagnostics when compared to rawinsonde observations for Melbourne (Table 2). Representations are significantly improved for wind diagnostics and diagnostics using a relatively small number of model levels, compared with column-integrated quantities and thermodynamic variables. For example, BARRA and ERA5 mean water vapor mixing ratio from 0 to 1 km above ground level (Qmean01), as well as the vertical wind shear from 0 to 6 km (S06), correlate better with observations (r = 0.902 and r = 0.933 for BARRA Qmean01 and S06, respectively) compared to mixed-layer convective available potential energy (MLCAPE; r = 0.562 for BARRA). Representations are also relatively poor for composite parameters which include multiple variables and may compound model errors for single variables. For example, the product of S06 and MLCAPE (MLCS6) has lower correlation (r = 0.542) compared to S06 and CAPE individually, with errors becoming even larger for diagnostics which use effective-layer ingredients such as the supercell composite parameter (SCP; r = 0.470), noting that skill degrades further when considering nonzero values only (Table 2). The variability in model bias between diagnostics will be discussed further (in section 3a) when interpreting diagnostic skill.

c. Grass pollen data

Pollen data are collected daily using a Burkard volumetric trap (Ong et al. 1995), located at the University of Melbourne (Fig. 1). For the case control analysis, data from the years 2009–17 are used, while counts from 1991 to 2018 are analyzed for long-term variability. It is noted that daily grass pollen counts are recorded for the 24 h to 1600 LT, while for the years 2017/18, pollen is recorded at 0900 (LT) the following day. For each case and control date, hospital data are compared with the grass pollen count from 24 h prior to measurement ($t - 1$), from 24 h after measurement ($t - 0$), and the maximum and total pollen counts over a 4-day window (using $t - 2$, $t - 1$, $t - 0$, and $t + 1$ recordings). All pollen measurements in this study are in units of grains m^{-3}.

d. Skill measures

Two different skill metrics are used to evaluate the ability of severe weather diagnostics in separating case and control days. These are the true skill statistic (TSS) and the critical success index (CSI). Each metric is calculated by comparing daily (maximum) meteorological data with case and control dates. The skill metrics are also calculated for grass pollen count data as an alternative predictor.

The TSS measures how well a diagnostic separates the case and control dates and uses all elements of the contingency table, such that it is insensitive to the proportion of cases and controls in the dataset. The TSS is given by

$$\mathrm{TSS} = \frac{\text{hits}}{\text{hits} + \text{misses}} - \frac{\text{false alarms}}{\text{false alarms} + \text{correct negatives}},$$

where the TSS ranges from −1 to 1, with a score of 0 representing no skill, and 1 representing a perfect separation of cases and controls. The CSI measures the fraction of cases that were correctly predicted by each diagnostic, and is given by

TABLE 1. Definitions of the severe weather diagnostics used in this study, as well as accompanying references.

	Description	Reference
BDSD	Brown and Dowdy (2021): Statistical diagnostic, based on fitting environmental variables from the BARRA and ERA5 reanalyses to severe convective wind events from station data using a stepwise forward variable selection algorithm: $\text{BDSD} = \frac{1}{1 + e^{-z}}$, where for BARRA: $z = 1.2(10^{-1})(\text{EBWD}) + 9.9(10^{-1})(\text{LR13}) + 2.1(10^{-1})(\text{Umean03}) + 2.4(10^{-4})(\text{MLEL}) + 2.0(10^{-2})(\text{RHMIN03}) - 1.2(10^{1})$ and for ERA5: $z = 6.1(10^{-2})(\text{EBWD}) + 1.5(10^{-1})(\text{Umean800–600}) + 9.4(10^{-1})(\text{LR13}) + 3.9(10^{-2})(\text{RHMIN13}) + 1.7(10^{-2})(\text{SRHE}) + 3.8(10^{-1})(Q_{\text{melting}}) + 4.7(10^{-4})(\text{LCL}) - 1.3(10^{1})$ and EBWD is the effective bulk wind difference (m s^{-1}) (Thompson et al. 2007), LR13 is the temperature lapse rate from 1 to 3 km above ground level (°C km^{-1}), Umean03 is the pressure-weighted mean wind speed from the surface to 3 km above ground level (m s^{-1}), Umean800–600 is the same but between the 800- and 600-hPa layers, MLEL is the equilibrium level using a mixed-layer parcel (m), RHMIN03 is the minimum relative humidity from the surface to 3 km above ground level (%), RHMIN13 is the same but between the 1- and 3-km levels, LCL is the lifting condensation level based on an effective-layer parcel (m), SRHE is the effective-layer storm relative helicity (m^2 s^{-2}) (Thompson et al. 2007) and Q_{melting} is the water vapor mixing ratio at the height of the melting level (g kg^{-1}).	Brown and Dowdy (2021)
DCAPE	Downdraft convective available potential energy. Calculated using pseudoadiabatic descent of a saturated convective air parcel, starting at the pressure level with minimum equivalent potential temperature (in the layer below 400 hPa above ground level).	Gilmore and Wicker (1998)
DCP	The derecho composite parameter: $\text{DCP} = \frac{\text{DCAPE}}{980\ \text{J kg}^{-1}} \times \frac{\text{MUCAPE}}{2000\ \text{J kg}^{-1}} \times \frac{\text{S06}}{20\ \text{kt}} \times \frac{\text{Umean06}}{16\ \text{kt}}$, where Umean06 is the pressure-weighted mean wind speed between the surface and 6 km above ground level, and other terms are defined in this table.	Evans and Doswell (2001)
GUSTEX	$\text{GUSTEX} = \alpha\text{WINDEX} + 0.5U_{500}$, where $\alpha = 0.6$, U_{500} is the wind speed at the 500 hPa (m s^{-1}), and WINDEX (McCann 1994) is defined as follows: $\text{WINDEX} = 5\left[H_m R_q(\tau^2 - 30 + q_1 - 2q_m)\right]^{0.5}$, where H_m is the height of the melting level (km), τ is the lapse rate from the surface to the freezing level (K km^{-1}), q_1 is the mean mixing ratio in the surface to 1-km layer (g kg^{-1}), q_m is the mixing ratio at the height of the melting level (g kg^{-1}) and $R_q = q_1/12$.	Geerts (2001)
MLCAPE	Mixed-layer convective available potential energy, where the starting parcel is defined using the mean conditions in the lowest 100 hPa above ground level.	—
MLCS6	The weighted product of MLCAPE and S06: $\text{MLCS6} = \text{MLCAPE} \times \text{S06}^{1.67}$	Brooks et al. (2003); Allen et al. (2011)
MUCAPE	Most-unstable convective available potential energy defined by the maximum CAPE in the vertical.	—

TABLE 1. (*Continued*)

	Description	Reference
MUCS6	The weighted product of MUCAPE and S06: $\text{MUCS6} = \text{MUCAPE} \times \text{S06}^{1.67}$	Brooks et al. (2003); Allen et al. (2011)
MWPI	Microburst wind speed potential index: $\text{MWPI} = \frac{\text{MLCAPE}}{1000\ \text{J kg}^{-1}} + \left\{ \frac{\tau}{5\ \text{K km}^{-1}} + \left[\frac{(T - T_d)_{850\text{hPa}} - (T - T_d)_{670\text{hPa}}}{5°\text{C}} \right] \right\}$ where τ is the lapse rate between the 850- and 670-hPa levels (K km^{-1}), T is air temperature (°C), and T_d is the dewpoint temperature (°C).	Pryor (2015)
Qmean01	Mass-weighted mean water vapor mixing ratio from the surface to 1 km above ground level	—
S06	Bulk vertical wind shear between the surface and 6 km above ground level (m s^{-1} unless stated otherwise)	—
SCP (fixed)	Supercell composite parameter (using a fixed layer wind shear term): $\text{SCP(fixed)} = \frac{\text{MUCAPE}}{1000\ \text{J kg}^{-1}} \times \frac{\text{SRH01}}{50\ \text{m}^2\ \text{s}^{-2}} \times \frac{\text{S06}}{20\ \text{m s}^{-1}}$, where SRH01 is storm relative helicity in the 0–1 km above ground level layer, assuming a left-moving storm, and other terms are defined elsewhere in this table. S06 is capped at 20 m s^{-1}, and the shear term is set to zero for values below 10 m s^{-1}.	Thompson et al. (2007)
SCP	Supercell composite parameter: $\text{SCP} = \frac{\text{MUCAPE}}{1000\ \text{J kg}^{-1}} \times \frac{\text{ESRH}}{50\ \text{m}^2\ \text{s}^{-2}} \times \frac{\text{EBWD}}{20\ \text{m s}^{-1}}$, where ESRH is storm relative helicity in the effective layer, assuming a left-moving storm, EBWD is the effective-layer bulk wind difference, and other terms are defined elsewhere in this table. EBWD is capped at 20 m s^{-1}, and the shear term is set to zero for values below 10 m s^{-1}.	Thompson et al. (2007)
T-Totals	Total totals: $\text{total totals} = T_{850\text{hPa}} + \text{DP}_{850\text{hPa}} - 2(T_{500\text{hPa}})$, where T is air temperature, and DP is the dewpoint temperature.	Miller (1972)
WG10	The parameterized model wind gust produced by BARRA and ERA5, defined as an hourly maximum.	Su et al. (2019); Hersbach et al. (2020)

$$\text{CSI} = \frac{\text{hits}}{\text{hits} + \text{misses} + \text{false alarms}},$$

ranging from 0 to 1, with a score of 1 representing perfect identification. As the CSI does not use the correct negatives from the contingency table, it provides complementary information to the TSS in that it is based on the predicted positives and missed events.

For each diagnostic, the TSS and CSI are calculated on 1000 linearly spaced thresholds ranging from the minimum to the 99.5th percentile, with respect to case and control dates. The scores reported here represent the optimal threshold which maximizes each skill metric over the range of thresholds considered for each diagnostic. For each optimized score, a two-tailed 95% confidence interval is calculated, which has been estimated by resampling the case and control dataset 1000 times, with replacement. The odds ratio (OR) is also calculated using optimal thresholds for key diagnostics, which is given by

$$\text{OR} = \frac{\text{hits} \times \text{correct negatives}}{\text{misses} \times \text{false alarms}},$$

and describes the ratio of the odds of a modeled event being observed to the odds of a modeled event not being observed, with values greater than 1 representing skillful event identification.

e. Climate driver analysis

The long-term relationship between days with high grass pollen, thunderstorm environments based on severe weather diagnostics, and large-scale climate drivers relevant for the region is investigated. This is done by computing the Pearson correlation coefficient between the number of days with a favorable atmospheric environment during the grass pollen season from ERA5 and BARRA (1991–2018), the number of days with high grass pollen concentrations, and seasonal mean climate driver indices. The method by which a favorable environment and high grass pollen day are identified is discussed in later sections and is informed by case/control results.

TABLE 2. An assessment of severe weather diagnostics from BARRA and ERA5 compared with rawinsonde data from Melbourne airport, in terms of Spearman's correlation coefficient (r), root-mean-square error (RMSE), and mean error (ME). Hourly BARRA and ERA5 data corresponding to the rawinsonde launch time are used, at the grid point closest to Melbourne airport (Fig. 1), with 1356 samples available over the 2009–17 period. Statistics are also given using only observed samples greater than zero for each diagnostic, which are listed in parentheses.

	BARRA			ERA5		
	r	RMSE	ME	r	RMSE	ME
BDSB	0.902 (0.902)	0.174 (0.174)	0.001 (0.001)	0.977 (0.977)	0.100 (0.100)	0.002 (0.002)
DCAPE	0.602 (0.602)	273.688 (273.688)	−134.064 (−134.064)	0.724 (0.724)	199.887 (199.887)	−87.447 (−87.447)
DCP	0.674 (0.567)	0.221 (0.267)	−0.003 (−0.007)	0.725 (0.637)	0.145 (0.177)	−0.014 (−0.021)
GUSTEX	0.902 (0.902)	4.754 (4.754)	0.087 (0.087)	0.939 (0.939)	3.703 (3.703)	−0.586 (−0.586)
MLCAPE	0.562 (0.513)	94.161 (149.722)	5.087 (9.191)	0.707 (0.653)	56.927 (93.406)	−3.434 (−11.458)
MLCS6	0.542 (0.446)	12 526.425 (20 687.471)	338.850 (517.098)	0.691 (0.602)	8673.943 (14 459.798)	−539.290 (−1672.190)
MUCAPE	0.713 (0.630)	196.118 (228.089)	6.741 (5.938)	0.773 (0.676)	139.213 (168.957)	−5.669 (−10.191)
MUCS6	0.694 (0.591)	25 081.654 (30 037.435)	269.722 (−23.789)	0.767 (0.682)	16 743.097 (20 359.957)	−566.607 (−1062.419)
MWPI	0.763 (0.608)	2.424 (1.911)	−1.250 (−0.609)	0.854 (0.757)	2.561 (1.500)	−1.561 (−0.531)
Qmean01	0.902 (0.902)	0.773 (0.773)	−0.214 (−0.214)	0.948 (0.948)	0.535 (0.535)	−0.121 (−0.121)
S06	0.933 (0.933)	3.222 (3.222)	−0.285 (−0.285)	0.960 (0.960)	2.428 (2.428)	−0.180 (−0.180)
SCP	0.470 (0.290)	0.410 (2.186)	0.023 (0.257)	0.555 (0.216)	0.264 (1.496)	0.0003 (−0.166)
SCP (fixed)	0.618 (0.428)	0.312 (0.423)	0.013 (0.017)	0.699 (0.533)	0.217 (0.297)	0.006 (0.006)
T-Totals	0.903 (0.900)	6.280 (5.687)	1.939 (1.678)	0.955 (0.954)	4.708 (4.265)	0.546 (0.366)
WG10	0.815 (0.815)	2.201 (2.197)	0.562 (0.558)	0.813 (0.812)	2.193 (2.193)	−0.469 (−0.471)

Correlations are calculated for El Niño–Southern Oscillation (ENSO; Niño-3.4 index from the U.S. National Weather Service Climate Prediction Center), Indian Ocean dipole (IOD; dipole mode index from the National Oceanographic and Atmospheric Administration Physical Sciences Laboratory), and southern annular mode (SAM; index from the British Antarctic Survey).

Historical trends are calculated by fitting a linear polynomial to the number of days per year with high grass pollen or a favorable thunderstorm environment to the number of years since 1991. Confidence estimates for climate driver correlations and long-term trends are estimated by randomly resampling the annual time series 1000 times with replacement.

3. Results

a. Case/control analysis

Out of the 15 convective variables tested from the BARRA atmospheric reanalysis (shown in Table 1), 14 are able to skillfully identify high-presentation asthma cases during the grass pollen season in Melbourne, as represented by having a TSS greater than 0 at a 95% confidence level (Table 3). This suggests that high-presentation asthma events during the grass pollen season are to some extent associated with conditions related to thunderstorm occurrences based on these cases. The same 14 variables are also shown as being significantly skillful using ERA5 data based on the TSS, with CSI results generally consistent between the two reanalyses (Table 3). Given that skill scores are largely insensitive to the choice of reanalysis, for the remainder of this case/control analysis the focus will be on BARRA results, which is related to the operational NWP models used in forecasting for this region, although ERA5 will also be shown in some cases for robustness.

The most skillful diagnostic from BARRA based on having an optimal TSS score of 0.541 and a CSI of 0.118 is the mean water vapor mixing ratio from the surface to 1 km above ground level (Qmean01). This skill is potentially due to enhanced levels of moisture in the lower troposphere providing a necessary ingredient for thunderstorms, by increasing the amount of convective available potential energy (CAPE) in an atmospheric column, which is consistent with a similar CSI for mixed-layer CAPE (MLCAPE; 0.113). However, the relatively low TSS for MLCAPE (0.461) suggests that there may be additional factors relating Qmean01 to high-presentation asthma occurrences, such as pollen rupturing due to high amounts of ML water (Taylor and Jonsson 2004). It is also possible that relatively high TSS scores for Qmean01 compared with MLCAPE is related to improved representation within the reanalysis models, with a correlation coefficient of 0.902 for Qmean01 when compared with rawinsonde data, and 0.562 for MLCAPE (Table 2). The results in Table 3 demonstrate that atmospheric conditions may be important for the identification of high-presentation asthma cases in this region, with the skill of Qmean01 greater than using pollen information over the 4-day window around each case/control date. For example, by applying an optimal threshold to the maximum pollen concentration over this window, a TSS of 0.492 and a CSI of 0.086 is reported (Table 3).

Relatively high skill in identifying high-presentation asthma cases is also achieved by composite thunderstorm diagnostics, such as the product of MLCAPE and vertical wind shear from 0 to 6 km (S06) raised to the power of 1.67 (MLCS6), with a TSS of 0.486 and CSI of 0.090. MLCAPE is used in this diagnostic for representation of a favorable thermodynamic profile for thunderstorm formation based on moisture availability and instability, with S06 representing sufficient changes in wind direction and/or speed with height to support

TABLE 3. The optimal true skill statistic (TSS) and critical success index (CSI) for severe weather diagnostics from the BARRA and ERA5 reanalyses and grass pollen concentrations, in relation to the identification of high-presentation asthma cases. See Table 1 for a description of each diagnostic. The 95% confidence interval (two-tailed) for each skill metric is also shown, attained by randomly resampling the case/control dataset 1000 times with replacement. The TSS values shown in italics represent skillful diagnostics (TSS above 0) as estimated by this approach.

	TSS (BARRA)	TSS (ERA5)	CSI (BARRA)	CSI (ERA5)
Qmean01	*0.541 [0.342, 0.730]*	*0.555 [0.340, 0.757]*	0.118 [0.053, 0.190]	0.127 [0.063, 0.194]
SCP	*0.517 [0.306, 0.731]*	*0.505 [0.293, 0.698]*	0.136 [0.071, 0.216]	0.123 [0.058, 0.206]
MLCS6	*0.486 [0.288, 0.643]*	*0.447 [0.225, 0.640]*	0.090 [0.042, 0.141]	0.109 [0.051, 0.174]
MLCAPE	*0.461 [0.260, 0.675]*	*0.408 [0.211, 0.622]*	0.113 [0.056, 0.176]	0.150 [0.051, 0.268]
MUCS6	*0.449 [0.237, 0.640]*	*0.438 [0.220, 0.609]*	0.064 [0.034, 0.097]	0.070 [0.034, 0.107]
BDSD	*0.432 [0.212, 0.608]*	*0.463 [0.258, 0.636]*	0.070 [0.027, 0.124]	0.089 [0.045, 0.138]
SCP (fixed)	*0.421 [0.196, 0.632]*	*0.448 [0.237, 0.653]*	0.075 [0.034, 0.126]	0.087 [0.041, 0.139]
DCP	*0.398 [0.202, 0.576]*	*0.419 [0.225, 0.585]*	0.064 [0.026, 0.107]	0.061 [0.033, 0.093]
MUCAPE	*0.382 [0.161, 0.583]*	*0.348 [0.130, 0.574]*	0.069 [0.016, 0.136]	0.092 [0.033, 0.159]
T-Totals	*0.368 [0.176, 0.549]*	*0.377 [0.155, 0.573]*	0.051 [0.026, 0.078]	0.071 [0.032, 0.117]
GUSTEX	*0.312 [0.281, 0.346]*	*0.317 [0.159, 0.462]*	0.047 [0.014, 0.083]	0.053 [0.022, 0.088]
WG10	*0.291 [0.085, 0.463]*	*0.302 [0.095, 0.483]*	0.040 [0.021, 0.060]	0.048 [0.011, 0.094]
S06	*0.266 [0.080, 0.438]*	*0.264 [0.078, 0.440]*	0.039 [0.018, 0.065]	0.038 [0.018, 0.064]
DCAPE	*0.238 [0.030, 0.420]*	*0.259 [0.052, 0.441]*	0.038 [0.017, 0.061]	0.049 [0.000, 0.101]
MWPI	0.149 [−0.056, 0.365]	0.134 [−0.085, 0.343]	0.038 [0.009, 0.078]	0.031 [0.016, 0.048]
	TSS	CSI		
Max pollen	*0.492 [0.286, 0.679]*	0.086 [0.045, 0.137]		
Pollen ($t-1$)	*0.445 [0.300, 0.557]*	0.097 [0.023, 0.180]		
Total pollen	*0.437 [0.241, 0.615]*	0.071 [0.032, 0.113]		
Pollen ($t-0$)	*0.267 [0.100, 0.406]*	0.038 [0.019, 0.058]		

organized convection. High values of S06 are often associated with synoptic-scale weather systems which frequently occur in southern Australia with potential to provide thunderstorm initiation (Pepler et al. 2020). The product of MLCAPE and S06 has been shown to relate to the occurrence of severe thunderstorms globally (Brooks et al. 2003), with a greater weighting of vertical wind shear (MLCS6) resulting in a stronger association with thunderstorm reports in Australia (Allen et al. 2011). Relatively high skill is also shown by the supercell composite parameter (SCP), with similar ingredients to MLCS6 but intended for rotating convective systems (Thompson et al. 2007), having a TSS of 0.517 and CSI of 0.136.

Based on optimizing the TSS, it appears that a Qmean01 value of around 10.4 g kg^{-1} from BARRA might provide an optimal discriminant for favorable meteorological conditions for this case dataset, while a threshold on the 4-day maximum grass pollen concentration of 78 m^{-3} might provide optimal identification using pollen information. Details on optimal univariate thresholds is presented in the appendix for all diagnostics (Table A1). The BARRA Qmean01 threshold of 10.4 g kg^{-1} is exceeded on 155 of the 828 case/control days, with 15 of these being cases ("hits") and the remaining 140 being controls ("false alarms"). Of the 673 days that did not exceed the 10.4 g kg^{-1} Qmean01 threshold, 6 were case days ("misses") with 667 controls ("correct negatives"). In terms of an odds ratio, this means that a day with Qmean01 greater than 10.4 g kg^{-1} is about 12 times more likely to represent a case day compared with a control day, compared with a maximum pollen threshold of 78 m^{-3} being 9 times more likely to represent a case day. The extent to which each of these variables separates case days from controls can be visualized in Fig. 2a, which shows daily maximum values of BARRA Qmean01 and 4-day maximum grass pollen relative to the univariate thresholds described above (10.4 g kg^{-1} for Qmean01 and 78 m^{-3} for grass pollen).

Figure 2 presents the joint distribution of Qmean01 and the 4-day maximum grass pollen concentration over all days in the study period (2009–17). Peak probabilities in both BARRA and ERA5 occur at Qmean01 values of 7–8 g kg^{-1}, with maximum grass pollen concentrations less than 40 m^{-3}. A large proportion of high-presentation asthma cases occur in a relatively low-frequency region of the joint distribution, with both high Qmean01 (greater than 10.4 g kg^{-1} for BARRA and 10.7 g kg^{-1} for ERA5) and pollen concentrations (greater than 78 m^{-3}). Also highlighted in Fig. 2 is the November 2016 event, which has relatively large values of Qmean01 and pollen concentrations but is not exceptional in terms of the joint distribution. The joint distribution of grass pollen and Qmean01 is generally consistent between BARRA and ERA5, with key differences being slightly higher median and 75th percentile values of Qmean01 in BARRA, and higher ERA5 Qmean01 values for case days resulting in a slightly higher optimal threshold using that dataset. Higher median values of BARRA daily maximum Qmean01 may result from a number of differences between the two reanalyses, including horizontal grid spacing, the number of pressure levels used to calculate the diagnostic or biases in upper-air or surface variables. It is noted that both reanalysis models are negatively biased when compared to rawinsonde observations (Table 2).

There is a weak positive correlation (Spearman's rank) of 0.22 (p value < 0.001) between daily Qmean01 values from

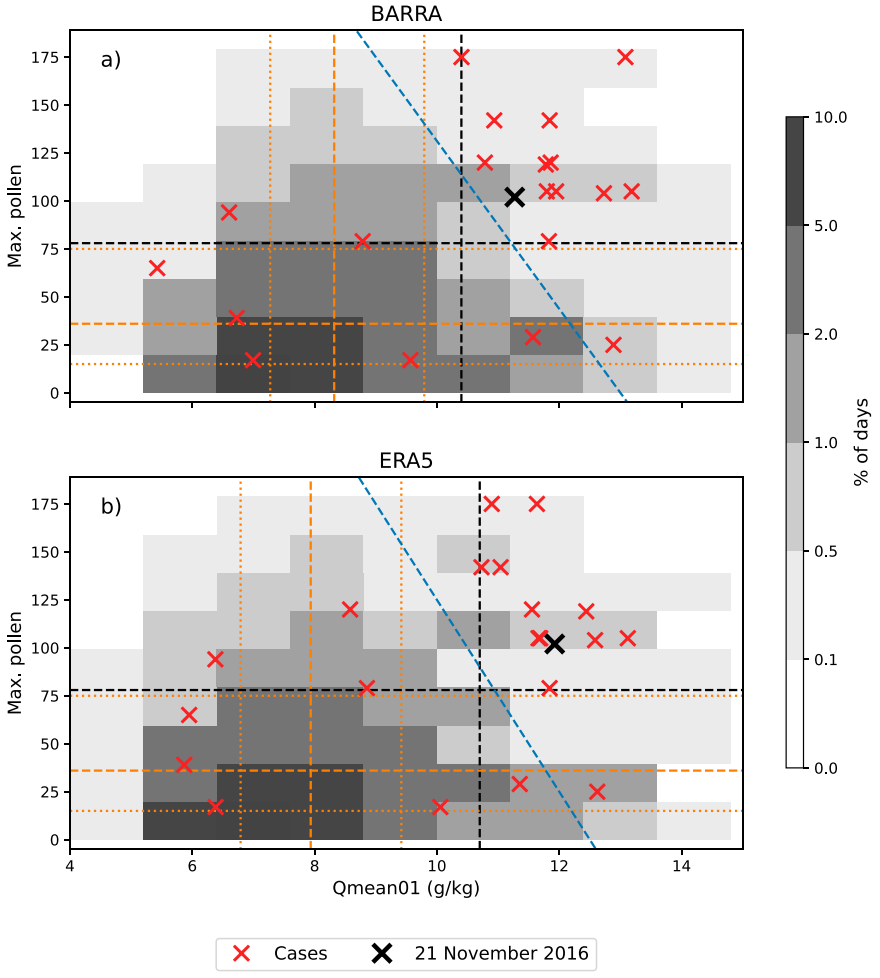

FIG. 2. The joint probability distribution of (a) BARRA and (b) ERA5 Qmean01 and the maximum 4-day grass pollen concentration (m^{-3}) for all days in the Melbourne grass pollen season over 2009–17 (1 Oct–31 Dec), shown as a percentage of all days (gray shading). Case dates are highlighted by red crosses, with the November 2016 case shown by a black cross, while dashed black lines show optimal univariate thresholds for separating case and control dates based on optimizing the TSS. Horizontal/vertical orange dashed/dotted lines represent the 25th, 50th, and 75th percentiles of Qmean01 and pollen using all days in the analysis period. Two-dimensional discriminant lines are shown by a dashed blue line, with details in appendix B.

BARRA and the maximum 4-day grass pollen concentration, with a stronger correlation using single-day pollen data on the day of each case/control date (0.39; p value < 0.001). As a result, the TSS for case identification was only slightly improved by combining univariate Qmean01 and grass pollen thresholds into a conditional multivariate threshold (TSS = 0.558). In addition, a significant improvement is gained in CSI from a reduced number of false alarms with the multivariate threshold (CSI = 0.186), but with only 13 correctly identified events compared with 15 using a univariate Qmean01 threshold. Similarly, false alarms are reduced by fitting a two-dimensional discriminant line to separate case and control dates, with a TSS of 0.566 and CSI of 0.137 for BARRA (Fig. 2). Details of the two-dimensional discriminants are shown in appendix B.

Sub-daily analysis of Qmean01 from BARRA reveals that on high-presentation asthma case days, favorable conditions gradually develop throughout the day, as indicated by mean values at each spatial point, with a peak at 2100 LT (Fig. 3). At this time, there is a high water vapor mixing ratio everywhere in the domain on average, including over both land and sea, with local minima over regions of high topography (see Fig. 1). On control days, the water vapor mixing ratio is much lower on average everywhere in the domain compared with case days, with increases over the land after around 1800 LT.

The results presented in this section suggest that daily maximum low-level water content is potentially important for epidemic asthma events, in combination with high grass pollen concentrations, and provides enhanced skill compared with measures of downdraft intensity as represented by regional

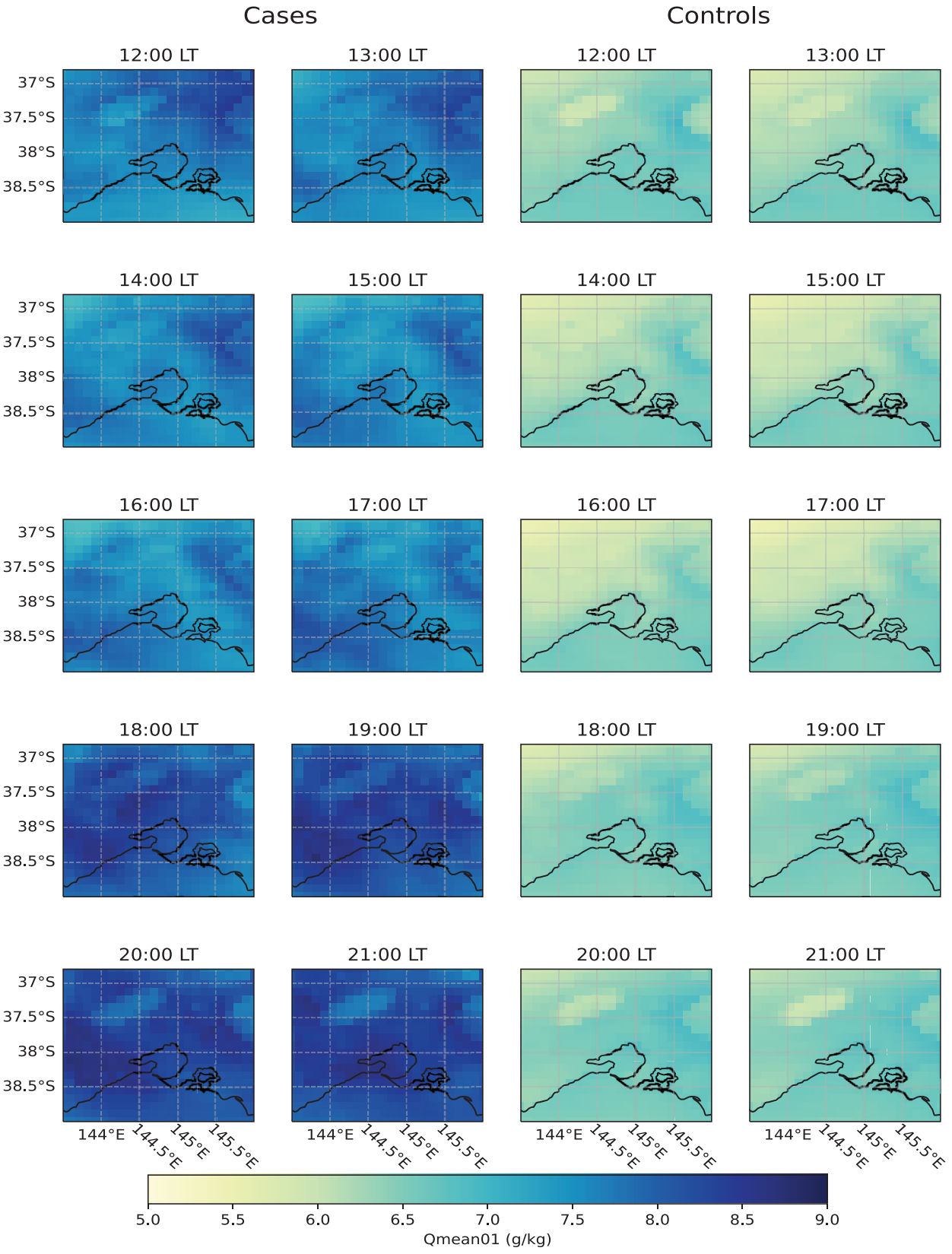

FIG. 3. The mean value for Qmean01 (left) over each case day and (right) control day, shown at each spatial point from BARRA at 10 instantaneous hourly times (from midday to 2100 LT).

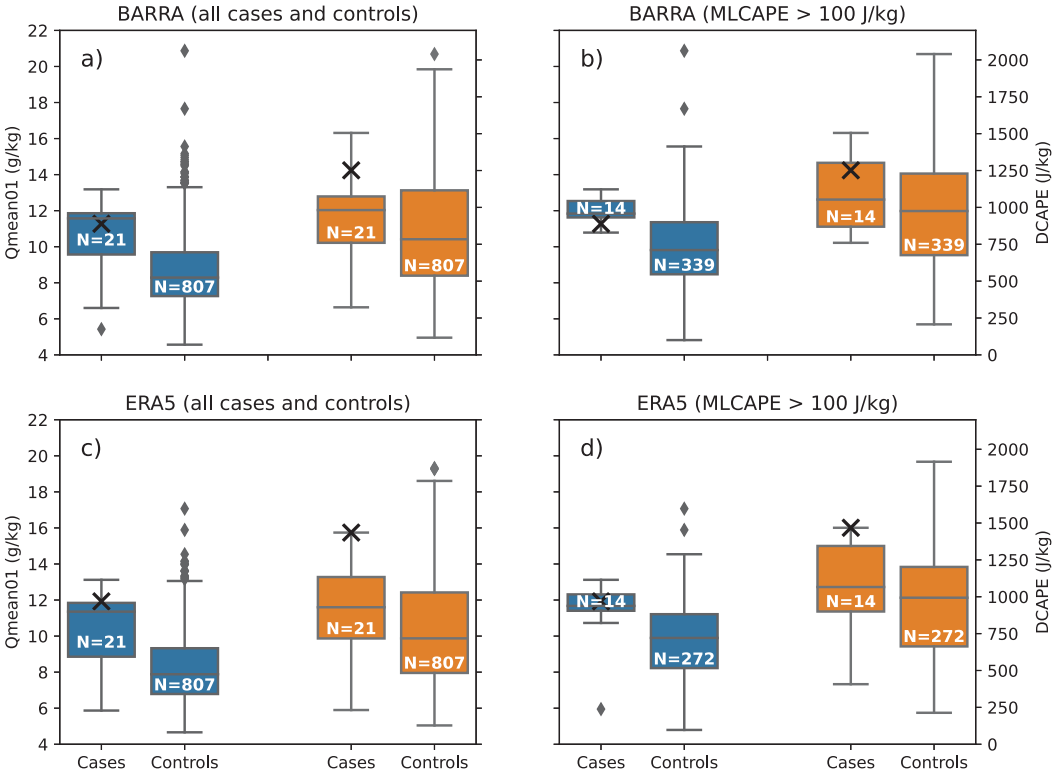

FIG. 4. The distribution of daily maximum Qmean01 (blue boxes) and DCAPE (orange boxes), shown separately for (a),(c) case and control days; (b),(d) conditionally unstable case and control days (defined by MLCAPE > 100 J kg^{-1}), and for (top) BARRA and (bottom) ERA5. Box ranges represent the lower to upper quartile of each distribution, with whiskers extending to 1.5 times the interquartile range, outliers highlighted by black diamonds, and median values shown by a horizontal line. The number of samples used for each distribution, *N*, is shown on each box. Values for the November 2016 case are shown by a black cross.

models such as the BDSD, GUSTEX, MWPI, and DCAPE diagnostics (see Tables 1 and 3). This result is in contrast with previous studies which have hypothesized that thunderstorm downdraft potential from the large-scale environment relates to epidemic asthma events, including Grundstein et al. (2017) who link the November 2016 Melbourne event to high values of DCAPE (Gilmore and Wicker 1998) from Global Forecasting System (GFS) model data (1252 J kg^{-1}). The distribution of Qmean01 and DCAPE is presented in Fig. 4 for the asthma case/control dataset, with a relatively large separation in the distribution of Qmean01 between case and control days compared with DCAPE. This is consistent between ERA5 and BARRA, and when considering conditionally unstable case and control days only (MLCAPE > 100 J kg^{-1}).

The analysis shown in Fig. 4 suggests that while environmental downdraft potential may be relevant for some thunderstorm asthma events (e.g., the November 2016 Melbourne event), it is not clear whether the downdraft diagnostics considered here can be systematically applied to identify relevant conditions. Large-scale low-level moisture content (represented here by Qmean01), which is potentially relevant for severe thunderstorms and pollen rupturing (Taylor and Jonsson 2004), may be more useful for systematic event identification using a regional model, based on the case/control dataset used here for Melbourne, Australia.

b. Long-term variability in meteorological conditions and high grass pollen concentrations

The interannual variability in days during the grass pollen season (1 October–31 December) with high 4-day maximum grass pollen concentrations and with high daily maximum Qmean01 is shown in Fig. 5 for 1991–2018. High grass pollen and Qmean01 days are defined using the thresholds presented in section 3b, which are 78 m^{-3} for grass pollen, 10.4 g kg^{-1} for BARRA Qmean01, and 10.7 g kg^{-1} for ERA5 Qmean01. Figure 5 shows that there is relatively large variability in days with high grass pollen concentrations, ranging from 0 days (2006, 2008, 2014, 2015) to 57 days per season (1996), with a strong negative trend of −1.16 days yr^{-1}, which has been shown previously for this dataset by de Morton et al. (2011), who suggested that long-term decreases could be due to decreasing rainfall in the region, as well as land use changes. The variability in days with high Qmean01 is much smaller, ranging from 26 to 3 days from the BARRA dataset and 18 to 1 days from ERA5, with both datasets showing positive trends of 0.42 and 0.24 days yr^{-1}.

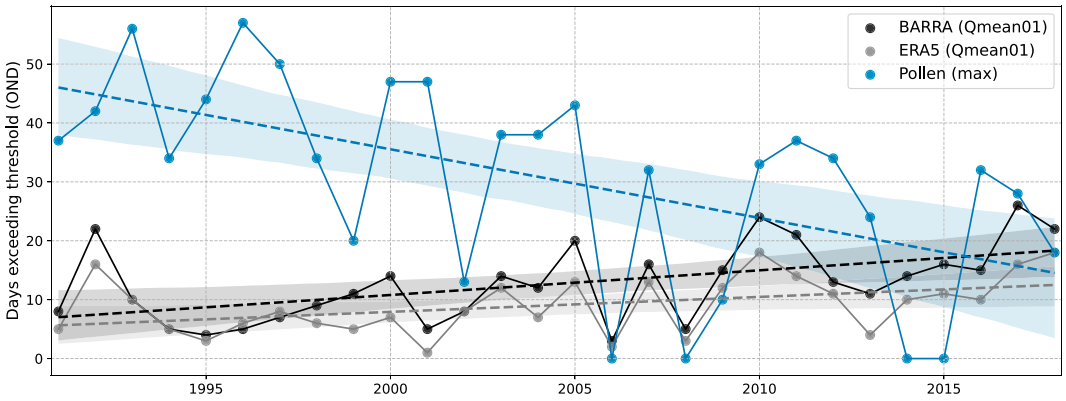

FIG. 5. Time series showing the number of days in the grass pollen season (1 Oct–31 Dec) exceeding thresholds for Qmean01 (10.4 g kg^{-1} for BARRA and 10.7 g kg^{-1} for ERA5) and 4-day maximum pollen concentrations (78 m^{-3}). A linear polynomial is fit to each time series and shown with a dashed line, with shading representing a two-sided 95% confidence interval based on a 1000-time random bootstrapping procedure.

The correlation between the annual number of days during the grass pollen season (1 October–31 December) with high Qmean01, grass pollen concentrations near Melbourne, and mean large-scale climate indices is shown in Table 4. Results suggest that the large-scale climate drivers examined here have little influence on the occurrences of high daily maximum Qmean01, which is potentially limited to a negative relationship with ENSO when considering BARRA data (p = 0.096). These results are broadly similar to previous studies examining the relationship between large-scale modes of variability and convective environments in this region (Allen and Karoly 2014; Dowdy 2020). However, correlations suggest that there may be a weak statistical relationship between high grass pollen days and the negative phases of SAM (p = 0.085), ENSO (p = 0.054), and the IOD (p = 0.029), which could potentially be driven by rainfall changes associated with each mode (Hendon et al. 2007; Risbey et al. 2009), noting that grass pollen concentrations in this region is also sensitive to a range of nonmeteorological factors (de Morton et al. 2011). It is noted that while there are some correlations between Qmean01 and grass pollen concentrations on daily time scales (section 3a), there is no significant correlation between annual occurrences of high Qmean01 and high grass pollen (Table 4).

4. Discussion and conclusions

Skillful identification of high-presentation asthma events is achieved using severe weather diagnostics derived from the BARRA atmospheric reanalysis for Melbourne, Australia. This is supported by similar results for the ERA5 global reanalysis and suggests that high-presentation asthma days within the grass pollen season in this region are related to thunderstorm conditions to some extent, with these conditions represented here using regional model data. The most skillful environmental diagnostic for the identification of epidemic asthma events out of the subset considered (Table 1), based on the CSI and TSS from BARRA-derived data, is Qmean01: the mean water vapor mixing ratio from the surface to 1 km above ground level. As well as being well represented compared to rawinsonde observations and relating to convective instability, high moisture content has been suggested by previous studies as a pollen rupturing mechanism (Taylor and Jonsson 2004). Therefore, there are physically plausible reasons why this diagnostic could relate to high-presentation asthma events, especially events induced by thunderstorm occurrences.

Qmean01 provides greater skill in indicating the occurrence of epidemic asthma cases than the use of grass pollen count data (shown by TSS and CSI scores in Table 3), suggesting that both the meteorological environment and pollen concentration are relevant factors. It is noted that pollen concentrations are positively correlated with Qmean01 for the case and control dates here, although this correlation is not observed on seasonal scales over a longer period. Around two-thirds of the high-presentation asthma cases used in this study occur in a relatively low-probability region of the Qmean01–pollen joint frequency distribution, and false alarms for the identification of high-presentation days can be reduced by using a multivariate

TABLE 4. The Pearson correlation coefficient between days in the grass pollen season (1 Oct–31 Dec) with high lower-tropospheric moisture (Qmean01) from BARRA and ERA5, high 4-day maximum pollen counts, and large-scale climate drivers (ENSO, SAM, and the IOD). The p values are shown in parentheses, based on a 1000-time bootstrapping estimate.

	BARRA (Qmean01 ≥ 10.4 g kg^{-1})	ERA5 (Qmean01 ≥ 10.7 g kg^{-1})	Pollen (≥78 m^{-3})
ENSO	−0.232 (0.096)	−0.0795 (0.326)	−0.302 (0.054)
SAM	0.212 (0.117)	0.141 (0.229)	−0.261 (0.085)
IOD	−0.0607 (0.371)	0.0264 (0.459)	−0.356 (0.029)
Pollen (≥78 m^{-3})	−0.0263 (0.438)	0.0196 (0.451)	—

Qmean01–pollen approach. Subdaily spatial analysis of hourly Qmean01 values composited over case and control days showed that low-level moisture is uniformly greater across the whole domain for the cases examined here relative to control dates, with increasing magnitudes throughout the day.

In addition to pollen rupturing due to high moisture, thunderstorms have also been hypothesized to induce epidemic asthma events through strong surface convergence due to downdrafts and outflows (Taylor and Jonsson 2004; Bannister et al. 2020). While storm-scale aspects such as downdrafts and surface convergence are not able to be represented by the regional and global reanalyses used here, it is noted that relatively low univariate skill was found using environmental measures specifically targeted at identifying strong thunderstorm downdrafts with associated severe wind gusts, for example the BDSB, GUSTEX, MWPI, WG10, and DCAPE diagnostics (see Tables 1 and 3, Fig. 4). The results presented here therefore suggest that while large values of downdraft potential diagnosed from the large-scale environment may be important for a subset of extreme epidemic asthma events (Grundstein et al. 2017), they are potentially unable to be used for systematic evaluation.

The long-term variability in favorable meteorological environments and 4-day maximum pollen concentrations during the grass pollen season (1 October–31 December) have also been investigated. Based on both BARRA and ERA5 data, there has been a significant increase in the frequency of high Qmean01 days from 1991 to 2018. Historical increases in near-surface moisture are expected from increasing global mean temperatures following the Clausius–Clapeyron relationship, and has been used by several studies to explain historical increases in severe thunderstorm environments, due to more frequently conditionally unstable convective environments (Mohr and Kunz 2013; Chen et al. 2020), noting that there are still large uncertainties associated with severe thunderstorm variability (Allen 2018). In contrast, decreasing frequencies of days with high grass pollen concentrations are reported here for Melbourne, which has been shown previously by de Morton et al. (2011). While that study explained a large amount of the long-term variability using rainfall decreases in the region, it also noted that nonmeteorological factors such as land-use changes are important for grass pollen variability, with future changes in pollen concentrations therefore highly uncertain (Beggs 2004).

Correlations between large-scale climate drivers and the occurrence frequency of high Qmean01 days reveal a limited relationship with the IOD, ENSO, or SAM during the grass pollen season, although negative correlations may exist between these climate drivers and days with high grass pollen. While rainfall in southeastern Australia is strongly modulated by these climate modes (Risbey et al. 2009), it appears the relationship is reduced for water vapor mixing ratio using the daily maximum point data considered here for Melbourne. An overall lack in association between Qmean01 and ENSO, SAM, and the IOD agrees with previous studies which have focused on thunderstorm environments in the Australia region (Allen and Karoly 2014; Dowdy 2020). In contrast, higher rainfall could relate to grass pollen concentrations through increased agricultural productivity in surrounding regions, noting a range of nonmeteorological factors also influence grass pollen concentrations (de Morton et al. 2011).

Based on this analysis for Melbourne, Australia, regional and global atmospheric models such as those used by the BARRA and ERA5 reanalyses can provide insight on environments which are relevant for high-presentation asthma days, with these events being associated with high amounts of low-level moisture, which in-turn could be associated with favorable thunderstorm environments and/or pollen rupturing mechanisms. This indicates that convection-parameterizing atmospheric models can complement the decision-making related to thunderstorm asthma forecasting in this region, and in particular their representation of low-level moisture content, based on historical events occurring with unusually high values for this region. Grass pollen concentrations and meteorological conditions both appear to be influential for epidemic thunderstorm asthma events based on the case and control dates examined here, confirming that both factors should receive significant weighting in operational decision-making. Future work could utilize these insights to further improve physical understanding and confidence for epidemic thunderstorm asthma warning services, while incorporating findings from previous studies which have demonstrated the importance of thunderstorm outflow and convergence, noting that environmental measures of strong thunderstorm downdrafts were not found by the current study to identify cases with a large amount of skill. It follows that insights on the role of surface convergence, including from thunderstorms and their related downdrafts, may be gained from convection-allowing models which can partially resolve thunderstorms and other mesoscale circulations.

Acknowledgments. This research was supported in part through the Climate Systems Hub of the National Environmental Science Program (NESP). Associate Professor Ed Newbigin kindly provided daily grass pollen counts measured at the University of Melbourne starting in 1991. We also acknowledge the Victorian Agency for Health Information for the provision of the de-identified hospital asthma presentation data used to identify case and control days. The project was approved by the Human Research Ethics Committee of the University of Melbourne (Approval 2056587.1). Reviews on earlier version of this manuscript by Tony Bannister and Samuel Bell from the Bureau of Meteorology are gratefully acknowledged.

Data availability statement. Hourly reanalysis data used to calculate severe weather diagnostics are openly available from the Australian National Computing Infrastructure (NCI) for BARRA (http://dx.doi.org/10.4225/41/5993927b50f53) and ERA5 (http://dx.doi.org/10.25914/5fb115b82e2ba). Hospital presentation data are from the Victorian Emergency Minimum Dataset, which is restricted; however, access can be applied for through the Victorian Department of Health and Human Services "HOSdata" website (https://www.bettersafercare.vic.gov.au/data-reports/datasets/hosdata-victorian-hospital-data-reports).

TABLE A1. Optimal thresholds for high-presentation asthma case identification relative to control days for diagnostics from BARRA and ERA5, as well as grass pollen data. Optimal thresholds are based on applying 1000 linearly spaced thresholds and maximizing the TSS and CSI for each diagnostic. For the TSS, a two-tailed 95% confidence interval is presented, based on randomly resampling the case/control dataset 1000 times with replacement and calculating the optimal diagnostic for each sample.

	TSS threshold (BARRA)	TSS threshold (ERA5)	CSI threshold (BARRA)	CSI threshold (ERA5)
Qmean01	10.397 [9.513, 11.556]	10.723 [8.575, 11.32]	11.777	10.89
SCP	2.645 [0.186, 3.689]	0.408 [0.068, 2.201]	3.614	2.201
MLCS6	25 847 [25 847, 107 557]	26 536 [9650, 79 608]	107 557	75 588
MLCAPE	865 [306, 991]	346 [28, 1050]	991	1167
MUCS6	239 898 [150 864, 272 049]	100 111 [63 095, 189 286]	239 898	176 667
BDSD	0.987 [0.922, 0.997]	0.971 [0.907, 0.998]	0.999	0.997
SCP (fixed)	2.974 [1.052, 4.576]	0.986 [0.397, 2.061]	4.576	2.046
DCP	0.641 [0.337, 2.866]	0.319 [0.3, 0.86]	2.866	0.628
MUCAPE	1852 [1421, 2577]	1108 [347, 2176]	5849	2025
T-Totals	50.9 [50.9, 53.0]	50.3 [49.4, 53.1]	52.1	53.0
GUSTEX	35.3 [35.2, 50.6]	38.7 [32.1, 50.1]	52.2	49.6
WG10	18.3 [16.0, 19.5]	15.3 [13.9, 19.2]	18.3	20.2
S06	26.9 [17.7, 34.0]	25.5 [16.5, 34.0]	33.7	31.7
DCAPE	758 [557, 1253]	732 [641, 1351]	981	1354
MWPI	5.742 [1.275, 9.295]	3.083 [−0.905, 4.194]	8.763	3.737
	TSS threshold (grass pollen)		CSI threshold (grass pollen)	
Max pollen	78.1 [37.1, 103.2]		98.0	
Pollen (t −1)	13.1 [13.1, 47.0]		97.0	
Total pollen	112.5 [36.2, 192.3]		186.0	
Pollen (t − 0)	7.1 [6.1, 19.0]		16.1	

Metadata for the pollen monitoring site at the University of Melbourne are published on the National Environmental Monitoring Sites Register (www. Neii.gov.au/viewer) and the original data are available on request (theteam@pollenforecast.com.au). Climate driver indices from the U.S. National Weather Service Climate Prediction Center are available online (https://www.cpc.ncep.noaa.gov/data/indices/) as are indices from the National Oceanographic and Atmospheric Administration Physical Science Laboratory (https://psl.noaa.gov/gcos_wgsp/Timeseries/) and British Antarctic Survey (https://legacy.bas.ac.uk/met/gjma/sam.html).

APPENDIX A

Optimal Diagnostic and Grass Pollen Thresholds

Table A1 presents optimal diagnostic thresholds for the identification of epidemic asthma cases used in this study. Thresholds are presented separately based on optimizing the TSS and CSI, and with diagnostics from both BARRA and ERA5 data.

APPENDIX B

Two-Dimensional Discriminants

Figure 2 is used to manually fit two-dimensional discriminant lines to the Qmean01–pollen (4-day maximum) joint distribution, in order to separate high-presentation asthma case and control dates. For BARRA, this discriminant line is given by

$$\text{Max pollen} + 43.75(\text{Qmean01}) \geq 568.75. \quad \text{(B1)}$$

And for ERA5

$$\text{Max pollen} + 50(\text{Qmean01}) \geq 625. \quad \text{(B2)}$$

These lines are shown on the joint distributions in Fig. 2 of the main text.

REFERENCES

Allen, J. T., 2018: *Climate Change and Severe Thunderstorms*. Oxford University Press, Vol. 1, https://doi.org/10.1093/acrefore/9780190228620.013.62.

——, and D. J. Karoly, 2014: A climatology of Australian severe thunderstorm environments 1979–2011: Inter-annual variability and ENSO influence. *Int. J. Climatol.*, **34**, 81–97, https://doi.org/10.1002/joc.3667.

——, ——, and G. Mills, 2011: A severe thunderstorm climatology for Australia and associated thunderstorm environments. *Aust. Meteor. Oceanogr. J.*, **61**, 143–158, https://doi.org/10.22499/2.6103.001.

——, ——, and K. J. Walsh, 2014: Future Australian severe thunderstorm environments. Part II: The influence of a strongly warming climate on convective environments. *J. Climate*, **27**, 3848–3868, https://doi.org/10.1175/JCLI-D-13-00426.1.

Anderegg, W. R. L., J. T. Abatzoglou, L. D. L. Anderegg, L. Bielory, P. L. Kinney, and L. Ziska, 2021: Anthropogenic climate change is worsening North American pollen seasons. *Proc. Natl. Acad. Sci. USA*, **118**, e2013284118, https://doi.org/10.1073/pnas.2013284118.

Bannister, T., and Coauthors, 2020: Are convergence lines associated with high asthma presentation days? A case-control study in Melbourne, Australia. *Sci. Total Environ.*, **737**, 140263, https://doi.org/10.1016/j.scitotenv.2020.140263.

——, and Coauthors, 2021: A pilot forecasting system for epidemic thunderstorm asthma in southeastern Australia. *Bull. Amer. Meteor. Soc.*, **102**, E399–E420, https://doi.org/10.1175/BAMS-D-19-0140.1.

Beggs, P. J., 2004: Impacts of climate change on aeroallergens: Past and future. *Clin. Exp. Allergy*, **34**, 1507–1513, https://doi.org/10.1111/j.1365-2222.2004.02061.x.

Bellomo, R., P. Gigliotti, A. Treloar, P. Holmes, C. Suphioglu, M. B. Singh, and B. Knox, 1992: Two consecutive thunderstorm associated epidemics of asthma in the city of Melbourne. The possible role of rye grass pollen. *Med. J. Aust.*, **156**, 834–837, https://doi.org/10.5694/j.1326-5377.1992.tb136994.x.

Blumberg, W. G., K. T. Halbert, T. A. Supinie, P. T. Marsh, R. L. Thompson, and J. A. Hart, 2017: Sharppy: An open-source sounding analysis toolkit for the atmospheric sciences. *Bull. Amer. Meteor. Soc.*, **98**, 1625–1636, https://doi.org/10.1175/BAMS-D-15-00309.1.

Brooks, H. E., J. W. Lee, and J. P. Craven, 2003: The spatial distribution of severe thunderstorm and tornado environments from global reanalysis data. *Atmos. Res.*, **67–68**, 73–94, https://doi.org/10.1016/S0169-8095(03)00045-0.

Brown, A., and Dowdy, A., 2021: Severe convection-related winds in Australia and their associated environments. *J. South. Hemisphere Earth Syst. Sci.*, **71**, 30–52, https://doi.org/10.1071/ES19052.

Chen, J., A. Dai, Y. Zhang, and K. L. Rasmussen, 2020: Changes in convective available potential energy and convective inhibition under global warming. *J. Climate*, **33**, 2025–2050, https://doi.org/10.1175/JCLI-D-19-0461.1.

Davies, J. M., B. Erbas, M. Simunovic, J. Al Kouba, A. Milic, and D. Fagan, 2017: Literature review on thunderstorm asthma and its implications for public health advice. Accessed 16 November 2021, https://www.health.vic.gov.au/publications/literature-review-on-thunderstorm-asthma-and-its-implications-for-public-health-advice.

de Morton, J., J. Bye, A. Pezza, and E. Newbigin, 2011: On the causes of variability in amounts of airborne grass pollen in Melbourne, Australia. *Int. J. Biometeor.*, **55**, 613–622, https://doi.org/10.1007/s00484-010-0361-x.

Doswell, C. A., and D. M. Schultz, 2006: On the use of indices and parameters in forecasting severe storms. *Electron. J. Severe Storms Meteor.*, **1** (3), https://ejssm.org/archives/2006/vol-1-3-2006/.

Dowdy, A. J., 2020: Climatology of thunderstorms, convective rainfall and dry lightning environments in Australia. *Climate Dyn.*, **54**, 3041–3052, https://doi.org/10.1007/s00382-020-05167-9.

Emmerson, K. M., and Coauthors, 2021: Atmospheric modelling of grass pollen rupturing mechanisms for thunderstorm asthma prediction. *PLOS ONE*, **16**, e0249488, https://doi.org/10.1371/journal.pone.0249488.

Evans, J. S., and C. A. Doswell, 2001: Examination of derecho environments using proximity soundings. *Wea. Forecasting*, **16**, 329–342, https://doi.org/10.1175/1520-0434(2001)016<0329:EODEUP>2.0.CO;2.

Geerts, B., 2001: Estimating downburst-related maximum surface wind speeds by means of proximity soundings in New South Wales, Australia. *Wea. Forecasting*, **16**, 261–269, https://doi.org/10.1175/1520-0434(2001)016<0261:EDRMSW>2.0.CO;2.

Gilmore, M. S., and L. J. Wicker, 1998: The influence of midtropospheric dryness on supercell morphology and evolution. *Mon. Wea. Rev.*, **126**, 943–958, https://doi.org/10.1175/1520-0493(1998)126<0943:TIOMDO>2.0.CO;2.

Grundstein, A., M. Shepherd, P. Miller, and S. E. Sarnat, 2017: The role of mesoscale-convective processes in explaining the 21 November 2016 epidemic thunderstorm asthma event in Melbourne, Australia. *J. Appl. Meteor. Climatol.*, **56**, 1337–1343, https://doi.org/10.1175/JAMC-D-17-0027.1.

Hendon, H. H., D. W. J. Thompson, and M. C. Wheeler, 2007: Australian rainfall and surface temperature variations associated with the Southern Hemisphere annular mode. *J. Climate*, **20**, 2452–2467, https://doi.org/10.1175/JCLI4134.1.

Hersbach, H., and Coauthors, 2020: The ERA5 global reanalysis. *Quart. J. Roy. Meteor. Soc.*, **146**, 1999–2049, https://doi.org/10.1002/qj.3803.

Ladwig, W., 2017: wrf-python (Version 1.3.2) [Software]. UCAR/NCAR, accessed 22 October 2021, https://doi.org/10.5065/D6W094P1.

Marks, G. B., J. R. Colquhoun, S. T. Girgis, M. Hjelmroos Koski, A. B. A. Treloar, P. Hansen, S. H. Downs, and N. G. Car, 2001: Thunderstorm outflows preceding epidemics of asthma during spring and summer. *Thorax*, **56**, 468–471, https://doi.org/10.1136/thx.56.6.468.

May, R. M., and Coauthors, 2019: MetPy: A Python Package for Meteorological Data (version 0.10.2). Unidata, accessed 22 October 2021, https://doi.org/10.5065/D6WW7G29.

McCann, D. W., 1994: WINDEX—A new index for forecasting microburst potential. *Wea. Forecasting*, **9**, 532–541, https://doi.org/10.1175/1520-0434(1994)009<0532:WNIFFM>2.0.CO;2.

Miller, R. C., 1972: Notes on analysis and severe-storm forecasting procedures of the air force global weather central. Tech. Rep. 200, Air Weather Service, 190 pp.

Mohr, S., and M. Kunz, 2013: Recent trends and variabilities of convective parameters relevant for hail events in Germany and Europe. *Atmos. Res.*, **123**, 211–228, https://doi.org/10.1016/j.atmosres.2012.05.016.

Ong, E. K., M. Singh, and R. Knox, 1995: Seasonal distribution of pollen in the atmosphere of Melbourne: An airborne pollen calendar. *Aerobiologia*, **11**, 51–55, https://doi.org/10.1007/BF02136145.

Pepler, A., A. Dowdy, P. van Rensch, I. Rudeva, J. Catto, and P. Hope, 2020: The contributions of fronts, lows and thunderstorms to southern Australian rainfall. *Climate Dyn.*, **55**, 1489–1505, https://doi.org/10.1007/s00382-020-05338-8.

Price, D., K. M. Hughes, F. Thien, and C. Suphioglu, 2021: Epidemic thunderstorm asthma: Lessons learned from the storm down-under. *J. Allergy Clin. Immunol.*, **9**, 1510–1515, https://doi.org/10.1016/j.jaip.2020.10.022.

Pryor, K. L., 2015: Progress and developments of downburst prediction applications of GOES. *Wea. Forecasting*, **30**, 1182–1200, https://doi.org/10.1175/WAF-D-14-00106.1.

Puri, K., and Coauthors, 2013: Implementation of the initial ACCESS numerical weather prediction system. *Aust. Meteor. Oceanogr. J.*, **63**, 265–284, https://doi.org/10.22499/2.6302.001.

Risbey, J. S., M. J. Pook, P. C. McIntosh, M. C. Wheeler, and H. H. Hendon, 2009: On the remote drivers of rainfall variability in Australia. *Mon. Wea. Rev.*, **137**, 3233–3253, https://doi.org/10.1175/2009MWR2861.1.

Schumacher, R. S., and K. L. Rasmussen, 2020: The formation, character and changing nature of mesoscale convective systems. *Nat. Rev. Earth Environ.*, **1**, 300–314, https://doi.org/10.1038/s43017-020-0057-7.

Sgarbossa, D., J. Fischer, M. Bass, S. Rennie, and J. Taylor, 2019: The end-to-end convective hazard risk forecast process developed by the Australian extreme weather desk for the South Australian 28 September 2016 tornado outbreak. *29th Conf. on Severe Local Storms*, Stowe, VT, Amer. Meteor. Soc., 128, https://ams.confex.com/ams/29SLS/webprogram/Paper355711.html.

Su, C.-H., and Coauthors, 2019: BARRA v1.0: The Bureau of Meteorology Atmospheric high-resolution Regional Reanalysis for Australia. *Geosci. Model Dev.*, **12**, 2049–2068, https://doi.org/10.5194/gmd-12-2049-2019.

Taszarek, M., J. T. Allen, M. Marchio, and H. E. Brooks, 2021: Global climatology and trends in convective environments from ERA5 and rawinsonde data. *npj Climate Atmos. Sci.*, **4**, 35, https://doi.org/10.1038/s41612-021-00190-x.

Taylor, P. E., and H. Jonsson, 2004: Thunderstorm asthma. *Curr. Allergy Asthma Rep.*, **4**, 409–413, https://doi.org/10.1007/s11882-004-0092-3.

Thien, F., and Coauthors, 2018: The Melbourne epidemic thunderstorm asthma event 2016: An investigation of environmental triggers, effect on health services, and patient risk factors. *Lancet Planet. Health*, **2**, e255–e263, https://doi.org/10.1016/S2542-5196(18)30120-7.

——, J. M. Davies, M. Hew, J. A. Douglass, and R. E. O'Hehir, 2020: Thunderstorm asthma: An overview of mechanisms and management strategies. *Expert Rev. Clin. Immunol.*, **16**, 1005–1017, https://doi.org/10.1080/1744666X.2021.1826310.

Thompson, R. L., C. M. Mead, and R. Edwards, 2007: Effective storm relative helicity and bulk shear in supercell thunderstorm environments. *Wea. Forecasting*, **22**, 102–115, https://doi.org/10.1175/WAF969.1.

Trapp, R. J., N. S. Diffenbaugh, H. E. Brooks, M. E. Baldwin, E. D. Robinson, and J. S. Pal, 2007: Changes in severe thunderstorm environment frequency during the 21st century caused by anthropogenically enhanced global radiative forcing. *Proc. Natl. Acad. Sci. USA*, **104**, 19 719–19 723, https://doi.org/10.1073/pnas.0705494104.

Wakimoto, R. M., 2001: Convectively driven high wind events. *Severe Convective Storms*, C. A. Doswell, Ed., Amer. Meteor. Soc., 255–298.

Weisman, M. L., and J. B. Klemp, 1982: The dependence of numerically simulated convective storms on vertical wind shear and buoyancy. *Mon. Wea. Rev.*, **110**, 504–520, https://doi.org/10.1175/1520-0493(1982)110<0504:TDONSC>2.0.CO;2.